

QUIET SUN MAGNETIC FIELD MEASUREMENTS BASED ON LINES WITH HYPERFINE STRUCTURE

J. SÁNCHEZ ALMEIDA¹, B. VITICCHI², E. LANDI DEGL'INNOCENTI³, AND F. BERRILLI²

Draft version September 6, 2018

ABSTRACT

The Zeeman pattern of Mn I lines is sensitive to hyperfine structure (HFS) and, because of this reason, they respond to hG magnetic field strengths differently from the lines commonly used in solar magnetometry. This peculiarity has been employed to measure magnetic field strengths in quiet Sun regions. However, the methods applied so far assume the magnetic field to be constant in the resolution element. The assumption is clearly insufficient to describe the complex quiet Sun magnetic fields, biasing the results of the measurements. The diagnostic potential of Mn I lines can be fully exploited only after understanding the sense and the magnitude of such bias. We present the first syntheses of Mn I lines in realistic quiet Sun model atmospheres. Plasmas varying in magnetic field strength, magnetic field direction, and velocity, contribute to the synthetic polarization signals. The syntheses show how the Mn I lines weaken with increasing field strength. In particular, kG magnetic concentrations produce Mn I $\lambda 5538$ circular polarization signals (Stokes V) which can be up to two orders of magnitude smaller than what the weak magnetic field approximation predicts. As corollaries of this result, (1) the polarization emerging from an atmosphere having weak and strong fields is biased towards the weak fields, and (2) HFS features characteristic of weak fields show up even when the magnetic flux and energy are dominated by kG fields. For the HFS feature of Mn I $\lambda 5538$ to disappear the filling factor of kG fields has to be larger than the filling factor of sub-kG fields. Since the Mn I lines are usually weak, Stokes V depends on magnetic field inclination according to the simple cosine law, a scaling that holds independently of the magnetic field strength. Atmospheres with unresolved velocities produce very asymmetric line profiles, which cannot be reproduced by simple one-component model atmospheres. Inversion techniques incorporating complex magnetic atmospheres must be implemented for a proper diagnosis. Using the HFS constants available in the literature we reproduce the observed line profiles of nine lines with varied HFS patterns. Consequently, the uncertainty of the HFS constants do not seem to limit the use of Mn I lines for magnetometry.

Subject headings: line: profiles – Sun: magnetic fields – Sun: photosphere

1. INTRODUCTION

When the polarimetric sensitivity and the angular resolution exceed the required threshold, magnetic signals show up almost everywhere on the solar photosphere. The signals in supergranulation cell interiors are particularly weak, however, most of the solar surface is in the form of cell interiors and, therefore, these weak signals probably set the total unsigned magnetic flux and magnetic energy existing in the photosphere at any given time (e.g., Unno 1959; Stenflo 1982; Yi et al. 1993; Sánchez Almeida 1998, 2004; Schrijver & Title 2003). The importance of these ubiquitous quiet Sun magnetic fields depends, to a large extent, on the magnetic field strengths characterizing them. For example, the magnetic flux and the magnetic energy scale as powers of the field strength, and the connectivity between photosphere and corona is probably provided by the magnetic concentrations with the largest field strengths (e.g., Domínguez Cerdeña et al. 2006a). Unfortunately, measuring quiet Sun magnetic field strengths is not a trivial task. All measurements are based on the residual polarization left when a magnetic field of complex topology is observed with finite angular resolution (e.g., Emonet & Cattaneo 2001; Sánchez Almeida et al. 2003; Trujillo Bueno et al. 2004). Measuring implies assuming

many properties of the unresolved complex magnetic field and, in doing so, the measurements become model dependent and prone to bias. Depending on the technique used for measuring, the real quiet Sun exhibits weak daG fields (e.g., Stenflo 1982; Faurobert-Scholl 1993; Bommier et al. 2005), intermediate hG fields (e.g., Lin & Rimmele 1999; Khomenko et al. 2003; López Ariste et al. 2006), or strong kG fields (e.g., Sánchez Almeida & Lites 2000; Lites 2002; Domínguez Cerdeña et al. 2003). Such discrepancies can be naturally understood if the true quiet Sun contains a continuous distribution of field strengths going all the way from zero to two kG. Different techniques are biased differently and, therefore, they tend to pick out a particular part of the distribution. This scenario is very much consistent with realistic numerical simulations of magneto-convection (Cattaneo 1999; Stein & Nordlund 2006; Vögler et al. 2005; Vögler & Schüssler 2007). In order to provide a comprehensive observational description of the quiet Sun magnetic field strengths, one has to combine different methods carefully chosen to have complementary biases. Then the full distribution can be assembled taking the biases into account (Domínguez Cerdeña et al. 2006a).

In an effort to complement the existing magnetic field strength diagnostic techniques, López Ariste et al. (2002) proposed the use of spectral lines whose Zeeman patterns are sensitive to hyperfine structure (HFS). The formalism to deal with the HFS of spectral lines in magnetic atmospheres was developed more than thirty years ago by Landi Degl'Innocenti (1975). According to such formalism, the polarization of the HFS lines vary with magnetic field

Electronic address: jos@iac.es, bartolomeo.viticchi@roma2.infn.it, landi@arcetri.astro.it, francesco.berrilli@roma2.infn.it

¹ Instituto de Astrofísica de Canarias, E-38205 La Laguna, Tenerife, Spain

² Dipartimento di Fisica, Università di Roma Tor Vergata, Via della Ricerca Scientifica 1, I-00133 Rome, Italy

³ Università degli Studi di Firenze, Dipartimento di Astronomia e Scienza dello Spazio, Largo E. Fermi 2, 50125 Firenze, Italy

strength very differently from the lines commonly used in solar magnetometry. This unusual behavior was invoked by López Ariste et al. (2002) when proposing the use of HFS Mn I lines as a diagnostic tool for magnetic field strengths. López Ariste and coworkers have applied the idea to measure magnetic field strengths in quiet Sun regions (López Ariste et al. 2006, 2007; Asensio Ramos et al. 2007). Since the number of observables is limited, they minimize the statistical error of the measurement by minimizing the number of free parameters to be tuned. Milne-Eddington atmospheres (ME) are used to synthesize the polarization of the lines. The magnetic field is assumed to be constant and, therefore, the measurements provide some kind of weighted average of the true field strengths existing in the resolution elements. As we pointed out above, the topology of the quiet sun magnetic field is complex, with a distribution of field strengths and polarities coexisting in a typical resolution element. Then the ill-defined average provided by the Mn I lines is expected to be biased toward a particular range of field strengths, as it happens with the rest of the quiet Sun measurements (e.g., the NIR Fe I lines overlook kG magnetic concentrations, Sánchez Almeida & Lites 2000, Socas-Navarro & Sánchez Almeida 2003; the traditional visible Fe I lines exaggerate the contribution of kG fields, Bellot Rubio & Collados 2003, Martínez González et al. 2006; the Hanle scattering polarization signals are not sensitive to hG and kG, Faurobert et al. 2001, Sánchez Almeida 2005). The bias presented by the HFS Mn I lines is so far unknown, and the existing and forthcoming measurements based on those lines will be fully appreciated only when the sources of systematic effects are properly acknowledged and quantified. In order to explore the magnitude and the sense of the expected effects, we undertake the synthesis of Mn I lines in a number of realistic quiet Sun atmospheres with complex magnetic field distributions. The main trends are presented here.

The paper is organized as follows. Section 2 describes the software developed to carry out the syntheses. First, a ME code is needed to compare our syntheses with the results in the literature. Then, a plane parallel one-dimensional (1D) code allows us to explore the influence of realistic thermodynamic conditions on the polarization of lines with HFS. Finally, a Micro-Structured Magnetic Atmosphere (MISMA) code provides additional realism to the modeling since it includes coupling between magnetic field strengths and thermodynamic conditions, magnetic fields varying along and across the line-of-sight (LOS), mixed polarities in the resolution element, etc. All these codes are based on the original FORTRAN routine written by Landi Degl’Innocenti (1978). The analysis is focused on the line most often used in observations, namely, Mn I $\lambda 5538$. We discuss its intensity and circular polarization, since the linear polarization signals are very weak and they remain undetected so far. Single component and multi-component syntheses of this line are described in § 3 and § 4, respectively. An exploratory attempt to consider unresolved mixed polarities and velocity fields is carried out in § 5. The polarization of other Mn I lines is also considered in § 6. The implications of these syntheses are discussed in § 7.

2. DESCRIPTION OF THE SYNTHESIS PROCEDURES

The synthesis of Stokes profiles has been carried out using three different approaches to solve the radiative transfer equa-

tion for polarized light,

$$\frac{d\mathbf{I}}{ds} = -\mathbf{K}(\mathbf{I} - \mathbf{S}), \quad (1)$$

where $\mathbf{I} = (I, Q, U, V)^\dagger$ is the column vector containing the Stokes parameters, $\mathbf{S} = (B_T, 0, 0, 0)^\dagger$ is the source vector with B_T the LTE source function, \mathbf{K} is the 4×4 absorption matrix and, finally, the variable of integration s corresponds to the length along the LOS. (For details on matrix elements and the rest of the equation, see Landi Degl’Innocenti 1976.) The three codes differ in the model atmosphere used to describe the photosphere. The first one solves equation (1) under ME hypothesis. The source function is assumed to vary linearly with the continuum optical depth τ . Then the radiative transfer equation admits an analytic solution involving the two coefficients of the source function ($B_T = B_0 + B_1\tau$) and the seven coefficients of the absorption matrix, which are assumed to be constant (see Landi Degl’Innocenti 1975; equation [14]). The second code solves equation (1) for one-dimensional (1D) atmospheres. Realistic temperatures, pressures and magnetic field vectors are considered, but they only vary along the LOS so that a single ray suffices to synthesize the spectrum. The third code solves a different version of equation (1). It is obtained by a spatial averaging under the MISMA hypothesis (Sánchez Almeida et al. 1996). It assumes the solar atmosphere to have inhomogeneities smaller than the photon mean-free-path whose details are washed out by the radiative transfer process. Only their average properties matter. The new equation to be solved is,

$$\frac{d\mathbf{I}}{ds} = -\langle \mathbf{K} \rangle (\mathbf{I} - \mathbf{S}'), \quad (2)$$

where $\mathbf{S}' = \langle \mathbf{K} \rangle^{-1} \langle \mathbf{K} \mathbf{S} \rangle$ is a mean source vector. The brackets in equation (2) denote average over a volume whose dimension along the LOS is of the order of the photon mean-free-path. As a result of the averaging, $\langle \mathbf{K} \rangle$ and \mathbf{S}' are slowly varying functions of s , with this slow variation accounting for the large scale structure in the atmosphere. Pursuing the idea that optically-thin details are irrelevant for the final spectrum, Sánchez Almeida (1997) puts forward a type of model MISMA made of distinct components with different temperatures, pressures and magnetic field vectors. The coexistence of different components imposes a number of physical constraints to be satisfied, in particular, the lateral pressure balance causes the magnetic field to be coupled with the thermodynamics (see the original reference for an exhaustive description). These model MISMA, with their constraints, provide the degree of realism required to carry out our exploratory work. Note that the model MISMA reproduce all kinds of Stokes profiles observed in the quiet Sun, including those with extreme asymmetries (Sánchez Almeida & Lites 2000; Socas-Navarro & Sánchez Almeida 2002; Domínguez Cerdeña et al. 2006b). Equation (1) is formally identical to equation (2). They are integrated using a predictor-corrector method with the variables equi-spaced in a fixed grid of atmospheric heights. As we mention in the introduction, the linear polarization signals Q and U are very weak, and we do not analyze them here despite the fact that they are synthesized together with I and V .

All the codes are based on the FORTRAN procedure HYPER by Landi Degl’Innocenti (1978) that computes the Zeeman pattern of any line with hyperfine structure. The pattern depends on the externally imposed magnetic field, to-

gether with a set of atomic parameters, namely, the hyperfine structure constants, the quantum numbers of the two levels involved in the transition, the relative isotopic abundance, and the isotope shifts. When the Zeeman splitting is comparable to the hyperfine structure splitting, the Stokes profiles are strongly disrupted showing typical hyperfine structure features. The pattern depends on the so-called hyperfine structure constants \mathcal{A} and \mathcal{B} , which account for the two first terms of the Hamiltonian describing the interaction between the electrons in an atomic level and the nuclear magnetic moment – \mathcal{A} corresponds to the magnetic-dipole coupling whereas \mathcal{B} describes the electric-quadrupole coupling. The constants \mathcal{A} and \mathcal{B} can be determined empirically or theoretically. The values of \mathcal{A} adopted for our Mn I syntheses are listed in Table 1. The table includes the appropriate references, which indicate that \mathcal{B} is negligible small in all cases.

2.1. Testing the codes

We carry out different types of tests using the line Mn I $\lambda 5538$ as target. Intensity profiles are compared with the unpolarized solar atlas. The syntheses are also compared with the (ME) Stokes profiles existing in the literature. The codes are cross-checked one with respect to another, and with existing synthesis codes that neglect the HFS. All these efforts are summarized next.

The first series of tests is based on non-magnetic atmospheres. We start by recovering the ME Stokes I profile in López Ariste et al. (2002, Fig.3) when using the appropriate ME parameters (López Ariste 2007, private communication). In addition, Fig. 1 shows a reasonable ME fit to the FTS solar spectrum (Neckel 1999) using a Doppler width $\Delta\lambda_D = 0.029$ mÅ, a damping constant $a = 0.3$, an absorption coefficient $\eta_0 = 2.7$, a source function given by $B_0 = 1.0$ and $B_1 = 1.1$, and the atomic parameters in Table 1. Figure 1 also includes a fit to the observed profile using the 1D code. The line is synthesized in the quiet Sun model atmosphere by Maltby et al. (1986) using the atomic parameters in Table 1. The fit was carried out by trial-and-error varying the velocity along the LOS, the macroturbulence (v_{mac} , set to 1.3 km s $^{-1}$), and the Mn abundance ($\log[\text{Mn}]$, set to 5.30 in the scale where $\log[H]=12$). The MISMA code was also tested against the observed Stokes I assuming the thermodynamic parameters of the model atmosphere to be given by the model quiet Sun in Sánchez Almeida (1997, § 4.1). As in the case of 1D atmospheres, the atomic parameters are those listed in Table 1, and we vary the velocity along the LOS, the macroturbulence ($v_{mac} = 1.5$ km s $^{-1}$), and the Mn abundance ($\log[\text{Mn}]=5.31$). One additional consistency test was carried out with the 1D code. We compare the synthesis obtained neglecting the hyperfine structure (i.e., imposing $\mathcal{A} = \mathcal{B} = 0$) with the intensity of the 1D code from which we inherited the absorption coefficient routines (Sánchez Almeida 1992, § 5). The profiles of the two syntheses are identical within the numerical precision.

The second series of tests refers to magnetic atmospheres. Employing the atomic parameters and the atmospheres described above, we include a constant magnetic field vector. We use three different magnetic field strengths, $B = 100$ G, 300 G, and 900 G, with the same inclination, $\theta = 60^\circ$, and azimuth, $\phi = 0^\circ$. The ME syntheses reproduce the Stokes profiles in Fig. 4 of López Ariste et al. (2002). Stokes V profiles synthesized with the three codes are shown in Fig. 2. The agreement between the syntheses supports their internal con-

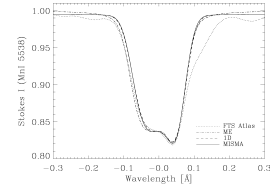


FIG. 1.— Mn I $\lambda 5538$ Stokes I profiles synthesized using the three codes and compared with the profile from the solar FTS atlas. The inset identifies the different codes and the observation. The wavelengths, in units of Å, are referred to the laboratory wavelength of the line. The profiles are normalized to the quiet Sun continuum intensity.

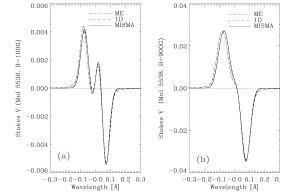


FIG. 2.— Mn I $\lambda 5538$ Stokes V profiles synthesized using the three codes with $B = 100$ G (a) and $B = 900$ G (b). The insets pair each type of line with the corresponding synthesis code. The profiles are normalized to the quiet Sun continuum intensity, and the wavelengths are referred to the laboratory wavelength of the line.

sistency – if the codes are tuned to produce similar Stokes I profiles (Fig. 1), then for the same field strength they also produce similar Stokes V (Fig. 2). The Stokes V profiles represented in Fig. 2 correspond to (and are consistent with) the two behaviors of Mn I $\lambda 5538$ described by López Ariste et al. (2002). The left panel in Fig. 2 shows the kind of profile for $B \lesssim 700$ G, with a characteristic reversal not far from the line core (hereafter HFS hump). Figure 2b corresponds to $B \gtrsim 700$ G, which do not generate HFS humps at the core. The presence or absence of such reversal is used by López Ariste and co-workers to distinguish between sub-kG fields (present) and kG fields (absent).

The results in § 6 can be regarded as a third independent test. The same non-magnetic quiet Sun model MISMA that reproduces the observed intensity of Mn I $\lambda 5538$ also accounts for eight additional Mn I lines with very different HFS patterns. Such agreement shows the realism and self-consistency of the syntheses.

3. SYNTHESSES OF Mn I $\lambda 5538$ IN 1D ATMOSPHERES

The weak magnetic field approximation is routinely used in solar magnetometry to, e.g., calibrate magnetograms. It is also valid for lines with HFS (Landi Degl’Innocenti 1975; Landi Degl’Innocenti & Landolfi 2004), and so it was used by López Ariste et al. (2006) to estimate the relative contribution of weak and strong fields to the observed quiet Sun signals. When the approximation holds the Stokes V profile is proportional to the longitudinal component of the magnetic field $B \cos \theta$,

$$V = -c \frac{dI}{d\lambda} B \cos \theta, \quad (3)$$

where the constant c depends on the particular spectral line, and the derivative of the intensity profile, $dI/d\lambda$, gives the variation with wavelength of Stokes V ⁴ (Landi Degl’Innocenti 1975;

⁴ Note, incidentally, that given the observed intensity profile of Mn I $\lambda 5538$ (Fig. 1), a hump at its Stokes V line core is unavoidable when

TABLE 1
ATOMIC PARAMETERS USED IN THE SYNTHESIS OF Mn I LINES

Line	Wavelength ^a [Å]	Transition ^a	χ^a [eV]	$\log gf$	g_{low}^a	g_{up}^a	\mathcal{A}_{low} [10^{-3}cm^{-1}]	\mathcal{A}_{up} [10^{-3}cm^{-1}]
Mn I $\lambda 4457$	4457.04	$z^6P_{5/2}^0 - e^6D_{3/2}$	3.073	-0.555 ^a	1.875	1.759	15.6 ^b	22.8 ^b
Mn I $\lambda 4470$	4470.14	$a^4D_{3/2} - z^4D_{3/2}^0$	2.940	-0.444 ^a	1.198	1.200	1.7 ^c	6.4 ^c
Mn I $\lambda 4502$	4502.22	$a^4D_{5/2} - z^4D_{7/2}^0$	2.919	-0.344 ^a	1.368	1.427	-4.6 ^c	1.5 ^c
Mn I $\lambda 4739$	4739.11	$a^4D_{3/2} - z^4F_{3/2}^0$	2.940	-0.490 ^a	1.198	0.400	1.7 ^c	22.3 ^c
Mn I $\lambda 5420$	5420.36	$a^6D_{7/2} - y^6P_{5/2}^0$	2.142	-1.460 ^a	1.584	1.886	13.5 ^d	-21.5 ^d
Mn I $\lambda 5516$	5516.77	$a^6D_{3/2} - y^6P_{3/2}^0$	2.178	-1.847 ^a	1.866	2.400	16.5 ^d	-31.5 ^d
Mn I $\lambda 5538$	5537.76	$a^6D_{1/2} - y^6P_{3/2}^0$	2.186	-1.920 ^e	3.327	2.400	27.8 ^d	-31.5 ^d
Mn I $\lambda 8741$	8740.93	$y^6P_{7/2}^0 - e^6D_{9/2}$	4.434	-0.05 ^f	1.712	1.554	-13 ^b	15.5 ^b
Mn I $\lambda 15262$	15262.70 ^g	$e^8S_{7/2} - y^8P_{5/2}^0$	4.889	+0.45 ^f	2.000	2.284 ^g	25.2 ^b	27.5 ^b

NOTE. — The symbols undefined in the main text stand for: lower-level oscillator strength gf , lower-level Landé factor g_{low} , upper-level Landé factor g_{up} , and lower-level excitation potential χ .

^a NIST Atomic Spectra Database, Ralchenko et al. (2007)

^b Lefèvre et al. (2003)

^c Blackwell-Whitehead et al. (2005)

^d Fisher & Peck (1939)

^e Margrave (1972)

^f Set to match the observed solar spectrum with $\log[\text{Mn}]=5.31$.

^g Asensio Ramos et al. (2007)

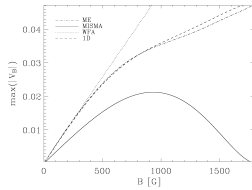


FIG. 3.— Maximum Stokes V amplitude as a function of the magnetic field strength for ME, 1D, and MISMA model atmospheres. The prediction corresponding to the weak field approximation is represented as the dotted line. All magnetic field inclinations are set to 60° . Magnetic field strengths are given in G.

Landi Degl’Innocenti & Landolfi 2004). We tested the approximation with the quiet Sun model atmospheres described in § 2.1, which are realistic in the sense that they reproduce the observed intensity profile when the magnetic field strength is close to zero (Fig. 1). The syntheses assume the magnetic field to be constant along the LOS, with the inclination θ set to 60° . Figure 3 shows the variation of the maximum Stokes V signal as a function of the magnetic field strength. The weak field approximation breaks down for fairly low magnetic field strengths, i.e., $B \gtrsim 400$ G (compare the dashed line and the dotted line in Fig. 3). Even more, the deviations are very important for kG magnetic field strengths. When the field strength is 1.5 kG the weak field approximation yields a Stokes V signal twice larger than the synthetic signals in 1D model atmospheres (Fig. 3). In order to test the dependence on $\cos\theta$ predicted by equation (3), we also carried out syntheses with various magnetic field inclinations. This dependence turns out to be closely followed by the synthetic signals, even for strong kG magnetic field strengths. The behavior was to be expected since Mn I $\lambda 5538$ is a weak line satisfying the weakly polarizing medium approximation (Sánchez Almeida & Trujillo Bueno 1999). In this approximation Stokes V scales with its specific absorption coefficient, which is proportional to $\cos\theta$ independently

$B \rightarrow 0$.

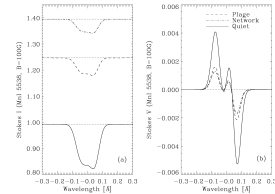


FIG. 4.— Stokes I and V profiles synthesized in three 1D model atmospheres corresponding to the quiet Sun (the solid line), a network region (the dotted dashed line), and a plage region (the dashed line). The magnetic field is constant with a strength of 100 G and an inclination of 60° . All profiles have been normalized to the quiet Sun continuum intensity. The dotted line is just a reference to show the continuum level.

of whether or no the spectral line has HFS.

The quiet Sun contains plasmas with all magnetic field strengths from 0 to 2 kG (§ 1). According to a mechanism originally put forward by Spruit (1976) and now well established, one expects a strong correlation between the magnetic field strength and the temperature of the observable photospheric layers. Plasmas having kG fields must be strongly evacuated to stay in mechanical balance within the photosphere. Consequently, strongly magnetized plasmas are transparent, showing light coming from deep and therefore hot (sub-)photospheric layers. In order to explore the dependence of the Mn I $\lambda 5538$ Stokes V signals on the thermodynamics, we compare synthetic profiles formed under different thermodynamic conditions but the same magnetic field strength. The line is synthesized in a quiet Sun model atmosphere (Maltby et al. 1986), a network model atmosphere (Solanki 1986; Solanki & Steenbock 1988), and a plage model atmosphere (Solanki 1986; Solanki & Steenbock 1988), with the temperature increasing from quiet Sun to network. The results are shown in Fig. 4. First note that the continuum intensity of Stokes I increases from quiet Sun (the coolest model) to network (the hottest model). In anticorrelation with continuum intensity, the Stokes V signals decrease with increasing temperature (Fig. 4, right). This behavior is not attributable to the HFS, but it is due to the ionization balance of Mn in

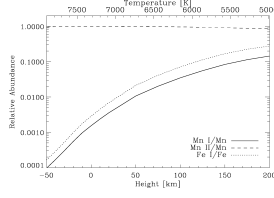


FIG. 5.— Relative abundance of Mn I and Mn II as a function of the height in the atmosphere for a quiet Sun stratification of temperatures. (The temperature corresponding to each height appears on the top of the figure.) The gas pressure is the same for all the heights, and it has been chosen to match the gas pressure of the non-magnetic quiet Sun some 100 km above the continuum optical depth equals one. The Fe I abundance is included for comparison – its overabundance with respect to Mn I is due to its higher ionization potential.

the photosphere. Mn I is the minor species so that a small modification of the ionization equilibrium does not alter the Mn II abundance but it drastically changes the number of Mn I atoms available for absorption. Increasing the temperature increases the ionization, and the Mn I lines weaken. Figure 5 shows the relative abundance of Mn I as a function of height in the atmosphere for a constant density representative of the layers where the lines are formed (say, 100 km above continuum optical depth equals one). According to Fig. 5, if the presence of a strong magnetic field decreases the formation height of a spectral line by 100 km, then the Mn I is depleted by more than one order of magnitude (compare the values at 100 km and 0 km). Note that this behavior is common to all Mn I lines, and it is also typical of other minor species like Fe I (e.g., the dotted line in Fig. 5). In short, the Mn I lines are expected to weaken with increasing magnetic field strength.

The coupling between magnetic field strength and temperature is fully accounted for in the MISMA syntheses, which partly explains the dimming of the kG Stokes V signals shown in Fig. 3 (the solid line). Another part of the dimming is due to non-magnetic plasma obscuring the magnetic plasma, and effect specific to MISMA and elaborated by Sánchez Almeida (2000).

4. MULTICOMPONENT SYNTHESIS OF Mn I λ 5538

The syntheses carried out so far assume very simple magnetic configurations. The magnetic field is either constant or, in the case of model MISMA, one magnetic component varies along the LOS. Due to the complex topology of the quiet Sun magnetic fields, our limited angular resolution, and the spatial averages carried out to obtain appropriate signals, those simplifications are insufficient to represent observed Stokes profiles. Real polarization signals are formed in plasmas having a range of magnetic properties, therefore, we improve the realism of the synthesis assuming multi-component model atmospheres. Specifically, we assume

$$I = \int_0^{B_{\max}} P(B) I_B dB, \quad (4)$$

and

$$V = \int_0^{B_{\max}} \langle \cos \theta \rangle P(B) V_B dB. \quad (5)$$

The symbols I_B and V_B represent the Stokes I and V profiles produced by an atmosphere with a single longitudinal magnetic field of strength B , whereas $P(B)$ stands for the fraction of resolution element occupied by such atmosphere. $P(B)$ is usually referred to as magnetic field strength probability density function (PDF). It is normalized to one, and it can be

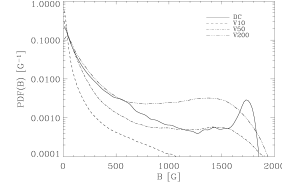


FIG. 6.— Magnetic field strength PDFs used for multi-component syntheses. The one labelled DC is from Domínguez Cerdeña et al. (2006a) while the V10, V50 and V200 are from Vögler (2003). See text for details.

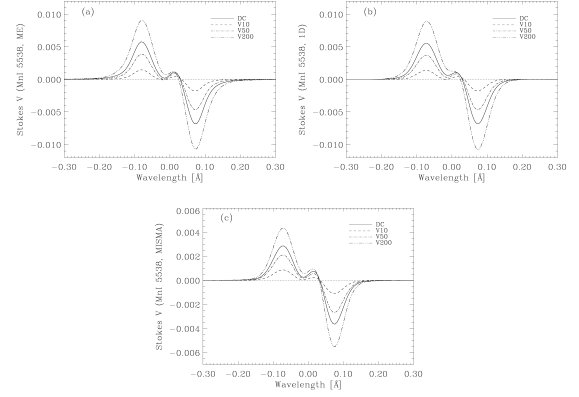


FIG. 7.— Multi-component Stokes V profiles synthesized using ME atmospheres (a), 1D atmospheres (b), and MISMA (c). The labels and the lines in the insets refer to the PDFs in Fig. 6. The profiles are normalized to the quiet Sun continuum intensity.

envisaged as the filling factor corresponding to each B . The maximum field strength existing in the quiet Sun sets B_{\max} to some 2 kG. As we show in Appendix A, equations (4) and (5) hold even for an arbitrary distribution of magnetic field directions, provided that the average inclination factor $\langle \cos \theta \rangle$ is computed properly. We would like to make it clear, however, that the PDF approach for representing the complications of the quiet Sun magnetic fields also has limitations. Equations (4) and (5) imply a one-to-one relationship between the magnetic field and the thermodynamic structure of the atmosphere. Although a coupling between magnetic field and thermodynamics is to be expected, the real relationship should have a significant scatter (e.g. Vögler 2003). Magnetic field variations along the LOS are restricted, and the overlapping along the LOS of structures with different magnetic fields is ignored. Our PDF approach is only a first approximation to the problem.

The four PDFs in Fig. 6 are used for synthesis. They correspond to one of the semi-empirical quiet Sun PDF obtained by Domínguez Cerdeña et al. (2006a) (labelled DC), plus the PDFs of the three magneto-convection numerical simulations by Vögler (2003), representing magnetic fluxes of 10 G, 50 G and 200 G (V10, V50 and V200, respectively). When ME atmospheres, 1D atmospheres, and model MISMA are combined according to these PDFs, one obtains the Stokes V profiles shown in Fig. 7. In this case the magnetic field inclination is constant and set to 60° , i.e., $\langle \cos \theta \rangle = 1/2$. The corresponding Stokes I profiles for the ME and the 1D cases are practically identical to those in Fig. 1. The MISMA synthesis has a continuum intensity 5% lower than that of the quiet Sun, since the thermodynamic structure of the model MISMA used for synthesis is cooler than the typical quiet Sun model atmospheres (see Fig. 11 in Sánchez Almeida & Lites 2000).

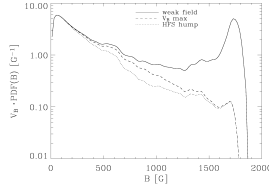


FIG. 8.— Relative contribution to the average Stokes V profile of a multi-component atmosphere characterized by the PDF labelled as DC in Fig. 6. The integral of the function represented in the plot is proportional to the Stokes V signal at a particular wavelength. The three curves correspond to any wavelength under the weak field approximation (the solid line), the wavelength where the average Stokes V signals is maximum (the dashed line), and the wavelengths where the HFS hump shows up (the dotted line). The units of the ordinates are relative since the curves have been scaled to the solid line when $B \rightarrow 0$.

Note that the Stokes V profiles in Figs. 7 always show HFS humps. This result warns us against simplistic interpretations of the presence of HFS features as the unequivocal signature of an atmosphere dominated by hG magnetic fields. Despite the fact that most of the atmospheric volume has very low field strengths, the magnetic flux and the magnetic energy of some of the PDFs used for synthesis are dominated by the tail of kG fields. The extreme case corresponds to V200 in Fig. 6, where 60% of the magnetic flux and 87% of the energy⁵ is in field strengths larger than 700 G, which is the field strength where the HFS hump disappears according to the ME syntheses. Even in this case the Stokes V profiles present clear HFS humps (see Fig. 7, the triple dotted-dashed lines). In order to understand this behavior one has to realize that the various magnetic field strengths existing in the atmosphere do not contribute to the *observable* signal in proportion to their magnetic flux, as expected if the weak magnetic field approximation would be satisfied (equation [3]). The strong kG fields are always under-represented (§ 3), and this bias is particularly severe at line center where the HFS hump shows up. The effect is shown in Fig. 8 which contains the integrand of equation (5) for one of the PDFs in Fig. 6 (DC). The integrand is given in three cases, (a) assuming the weak field approximation to hold (the solid line), (b) at the wavelength where the average Stokes V is maximum (the dashed line), and (c) at the line core (the dotted line). The individual spectra have been synthesized in model MISMA, but the qualitative behavior is common to all other model atmospheres. According to Fig. 8 the contribution of the kG fields to the HFS hump of the average Stokes V signal is some ten times smaller than that predicted by the weak field approximation. The relative contribution of the various field strengths to the hump is worked out as part of § 4.1.

4.1. On the diagnostic provided by the HFS hump

The observations of Mn I $\lambda 5538$ analyzed in the literature employ single component ME atmospheres (see § 1). The observed Stokes V profiles are fitted with synthetic profiles to obtain mean magnetic field strengths. In order to explore the diagnostic content of such inversion technique when applied to complex magnetic atmospheres, we developed a simple least squares minimization procedure to fit single-component ME profiles V_B to the synthetic multi-component V . The procedure fits

$$V = \alpha_B V_B, \quad (6)$$

⁵ Following Sánchez Almeida (2004) and Domínguez Cerdeña et al. (2006a), the unsigned magnetic flux and the magnetic energy are computed as the two first moments of the PDF.

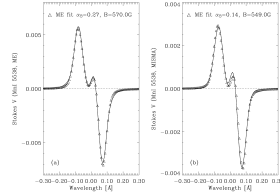


FIG. 9.— Least squares fits of Stokes V profiles synthesized in multi-component atmospheres (the solid lines) using single-component ME atmospheres (the symbols). (a) The multi-component Stokes V profile is synthesized in ME atmospheres. (b) The multi-component Stokes V profile is synthesized in model MISMA. The values for α_B and B retrieved from the fits are included in the figures. The two synthetic profiles correspond to the same PDF (DC). The profiles are normalized to the quiet Sun continuum intensity.

where the factor α_B and the field strength B are the only two unknowns. Figure 9 shows the single-component ME fit of the multi-component Stokes V produced by the DC PDF. In the case that the syntheses are based on ME atmospheres (Fig. 9a), the match is excellent. If the synthesis is based on model MISMA, the fit worsens a bit but still the agreement is fair (Fig. 9b). In both cases the field strength resulting from the ME *inversion* is about 550 G. We have unsuccessfully tried to link this average magnetic field strength with a particular property of the underlying PDF (the solid line in Fig. 6). It is neither the unsigned flux (~ 150 G) nor the most probable field strength (~ 13 G). Figure 8, the solid line, shows $BP(B)$, i.e., the unsigned flux per unit of magnetic field strength. It peaks at 50 G and 1700 G which, again, do not seem to bear any obvious relationship with the average ME magnetic field strength (~ 550 G).

In order to understand the relationship between the HFS hump and the magnetic fields existing in the multi-component atmosphere, we adopt a strategy avoiding ME fits. The presence or absence of a hump is certainly associated with the balance between weak fields and strong fields, but it is unclear how the hump is related with the fraction of atmosphere filled by weak and strong fields. One can quantify the presence of the hump using the derivative of the Stokes V profile at a wavelength λ_c slightly bluewards of the HFS maximum (i.e., centered in linear growth that ends up in the hump; see Fig 2a where $\lambda_c \simeq 0$). Then the sign of

$$\left. \frac{dV}{d\lambda} \right|_{\lambda_c}, \quad (7)$$

indicates the presence (> 0) or absence (< 0) of a hump⁶. According to equation (5),

$$\left. \frac{dV}{d\lambda} \right|_{\lambda_c} = \int_0^{B_{\max}} \langle \cos \theta \rangle P(B) \left. \frac{dV_B}{d\lambda} \right|_{\lambda_c} dB, \quad (8)$$

so the slope of the mean Stokes V is just a weighted mean of the slopes that characterize each field strength. Consequently, $dV_B/d\lambda|_{\lambda_c}$ yields the contribution of each field strength to the sign of the mean profile or, in other words, it yields the contribution of each field strength to the presence or absence of a hump in the average profile.

We have applied equation (8) to understand the HFS humps of the synthetic profiles in Fig. 7. Figure 10a shows the Stokes V derivative at line core ($\lambda_c = 0$) for the ME, the 1D and the MISMA model atmospheres. The magnetic field strength

⁶ This criterion assumes positive magnetic polarity, implying a positive Stokes V blue lobe. The same rule applies to negative polarity if one reverses the sense of the inequalities.

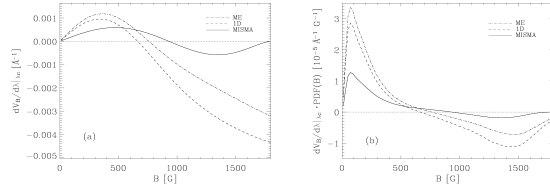


FIG. 10.— (a) Sensitivity of the HFS hump to the distribution of magnetic field strengths in the resolution element. The hump appears or goes away depending on the integral of $dV_B/d\lambda|_{\lambda_0}$ weighted with the PDF. The three curves correspond to the three model atmospheres used for multi-component synthesis (see the inset). (b) The derivative shown in (a) weighted with the V200 PDF. The integral is positive meaning that the resulting Stokes V profiles have HFS humps; see the triple dotted-dashed lines in Fig. 7.

where this derivative is zero indicates when V_B changes from having to lacking of a hump. As the figure shows, this transition field strength depends on the model atmosphere. The positive and negative lobes of the curves in Fig. 10a have similar amplitudes, which indicates that for the average Stokes profile to lack of a hump, the filling factor of the kG fields in the atmosphere has to be similar to the filling factor in weak fields. The requirement is not fulfilled by the PDFs in Fig. 6, whose filling factors are dominated by weak fields. Such superiority explains why all profiles in Fig. 7 show HFS humps. Equation (8) also explains why the magnetic flux in the form of kG structures has to exceed by far the flux in weak fields for the HFS hump to disappear. The HFS hump goes away when weak fields and strong fields have similar filling factors, but then the kG fields dominate the flux since the (unsigned) magnetic flux scales as the filling factor times the field strength. For example, consider a resolution element filled half-and-half with structures of 100 G and 1 kG. The HFS hump is not present, but the magnetic flux in kG fields is ten times the weak field flux.

Among the three curves in Fig. 10a, the one corresponding to MISMA reflects the solar conditions best, since it includes the dimming of the line with increasing field strength. This curve has positive and negative lobes of approximately the same area, therefore, the presence-absence of HFS humps in the Mn I $\lambda 5538$ Stokes V profiles is controlled by the fraction of photospheric atmosphere with field strengths smaller-larger than some 1 kG (i.e., the zero crossing point of the curve). Interpreting real observations with this rule-of-thumb requires disregarding the atmospheric volume having very weak magnetic fields, which produce no polarization and therefore do not contribute to the observed signal (see Fig 10b).

5. MIXED POLARITIES AND UNRESOLVED VELOCITIES

We expect the quiet Sun resolution elements to contain mixed polarities (Sánchez Almeida & Lites 2000; Socas-Navarro & Sánchez Almeida 2002), which leads to a reduction of the Stokes V signals. In the multi-component approximation parlance (equation [5]), having unresolved mixed polarities implies,

$$\langle \cos \theta \rangle \ll \langle |\cos \theta| \rangle, \quad (9)$$

since positive and negative $\cos \theta$ tend to cancel when carrying out the averages. If the positive polarity ($\cos \theta > 0$) and the negative polarity ($\cos \theta < 0$) have the same distribution of inclinations but they fill different fractions of resolution element, then

$$\langle \cos \theta \rangle = \langle |\cos \theta| \rangle (2f - 1), \quad (10)$$

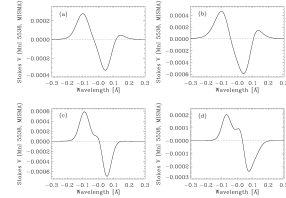


FIG. 11.— Examples of Stokes V profiles synthesized in semi-empirical model MISMA having unresolved mixed polarities correlated with velocities. They correspond to different classes in Sánchez Almeida & Lites (2000) – (a) class 6, (b) class 9, and (c) class 7. (d) Offspring of the class 7 model atmosphere where the two polarities have the same sign and the velocity difference has been increased. The profiles are normalized to the quiet Sun continuum intensity.

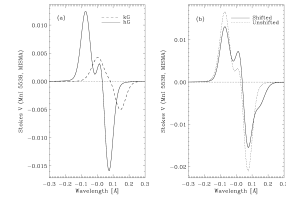


FIG. 12.— Two component Stokes V synthesis of weak and strong fields having different Doppler shifts. The strong fields are blueshifted with respect to the weak fields – see (a). The sum of the profiles in (a) leads to the profiles in (b), the solid line. If the relative Doppler shift is not considered, then the average Stokes V corresponds to the dotted line in (b). The profiles are normalized to the quiet Sun continuum intensity.

with f the fraction filled by the magnetic fields of positive polarity. If f does not depend on the magnetic field strength, the effect of mixed polarities is only a global scaling of the Stokes V profile with no effect on Stokes I (equations [4], [5], and [10]). However, the above view of the effect produced by unresolved mixed polarities is too simplistic. It implicitly neglects the existence of unresolved velocities in the resolution element coupled with changes of polarity. When the sense of the velocity and the polarity are correlated, the Stokes V of opposite polarities are Doppler shifted. They do not perfectly cancel, leaving observable residuals. Such coupling has been observed in Fe lines, and it produces very asymmetric Stokes V profiles (Sánchez Almeida & Lites 2000). In order to illustrate the effect, Fig. 11 shows Stokes V profiles of Mn I $\lambda 5538$ synthesized in empirical model MISMA with mixed polarities and different velocities (Sánchez Almeida & Lites 2000).

Velocities and other magnetic quantities are also expected to be coupled. For example, strong kG fields appear in intergranular lanes with downflows, whereas weak fields prefer granules with upflows (e.g., Cattaneo 1999; Socas-Navarro et al. 2004). This combination of Doppler shifts and magnetic field strengths renders profiles like the two component average shown in Fig. 12b, the solid line. It corresponds to the sum of the profiles in Fig. 12a, which are shifted by some 3.5 km s^{-1} . The HFS hump now appears elevated from the zero level, and the Stokes V blue wing is broadened with a conspicuous double absorption structure. These two features are common among the observed Stokes V profiles of Mn I $\lambda 5538$ (López Ariste et al. 2006, Figs. 8 and 9). The same features appear in the MISMA synthesis of Fig. 11d.

In short, mixed polarities and velocity gradients are properties of the real quiet Sun magnetic fields that affect the observed polarization in a significant way. They are not easy to deal with but must be taken into account for a realistic inter-

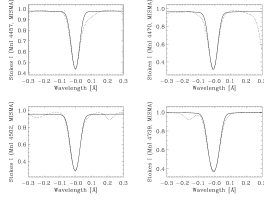


FIG. 13.— Mn I lines without obvious HFS features in the observed solar spectrum. The solid lines show our syntheses whereas the dotted lines correspond to the solar atlas (Neckel 1999). Wavelengths, given in Å, are referred to the laboratory wavelength of the lines. Each line is identified by the wavelength in the label of the ordinate axis. The profiles are normalized to the quiet Sun continuum intensity.

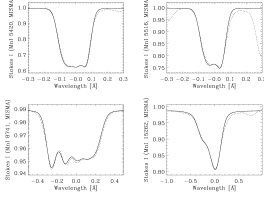


FIG. 14.— Mn I lines with HFS features. The solid lines correspond to our syntheses whereas the dotted lines show the solar atlas (Neckel 1999). Wavelengths, given in Å, are referred to the laboratory wavelength of the lines. Each line is identified by the wavelength in the label of the ordinate axis. The profiles are normalized to the quiet Sun continuum intensity.

pretation of the observations.

6. SYNTHESIS OF OTHER Mn I LINES

The purpose of synthesizing Mn I lines different from Mn I 5538 is threefold. First, it confirms that our LTE syntheses reproduce all kinds of observed HFS patterns. Second, it offers a chance to explore whether other Mn I lines show a sensitivity to magnetic fields complementary to Mn I 5538. Finally, it proves that the uncertainty of the HFS constants do not limit the use of Mn I lines for magnetometry.

All the syntheses in this section employ the non-magnetic quiet Sun MISMA that reproduces the Mn I 5538 profile in Fig. 1. Varying the macroturbulence and, in some cases also tuning the oscillator strength, we managed to fit the observed Stokes I profiles of all the lines we tried⁷. A total of eight Mn I lines reproduced by the code are shown in Figs. 13 and 14. They are split in two sets; Fig. 13 includes lines without obvious HFS features in the observed solar spectrum, whereas Fig. 14 shows lines with varied and assorted HFS. The agreement between the synthetic profiles and the solar atlas is good, an impression reinforced by the fact that the HFS constants determining the HFS patterns have not been tuned, but they come directly from the literature (Table 1).

The dependence of the various lines on magnetic field strengths has been studied by synthesizing them in the magnetic quiet Sun model MISMA used in § 4, increasing the field strength from ~ 100 G to ~ 2000 G. All the lines share a common behavior – they weaken with increasing field strength, and the HFS features tend to disappear. This behavior is also shared by the near IR line Mn I 15262 recently pointed out by Asensio Ramos et al. (2007) – Fig. 14, bottom right. On

⁷ The pattern of Mn I 5407 puzzled us for some time. As suggested by R. Manso, it turned out to be a blend of the Mn I line with two fairly strong Fe I lines that remain unidentified in the classical list by Moore et al. (1966), and which do not appear in the NIST Atomic Spectra Database. We found them with approximately the observed strengths among the list of lines by Kurucz at <http://kurucz.harvard.edu/line-lists.html>.

top of this general trend, and depending on the actual HFS constants, the Stokes V profiles of different lines present specific features. The line Mn I 5516 behaves like Mn I 5538, with a single HFS reversal at the line core. Then it is possible to relate the presence or absence of the hump with the distribution of field strengths in the atmosphere, exactly as the analysis carried out in § 4.1. The patterns of Mn I 5420 and Mn I 8741 are more complicated, and we have not been able to agree on a particular feature of the Stokes V profiles that can be treated as in § 4.1.

7. DISCUSSION AND CONCLUSIONS

The Zeeman pattern of the Mn I lines depends on hyperfine structure (HFS), which confers them a sensitivity to hG magnetic field strengths different from the lines traditionally used in solar magnetometry. This peculiarity has been used to measure magnetic field strengths in quiet Sun regions (see § 1). The methods applied so far assume the magnetic field strength to be constant in the resolution element, an approximation driven by feasibility rather than based on physical or observational arguments. Actually, it is not a good approximation since the magnetic fields of the quiet Sun are expected to vary on very small spatial scales, with field strengths spanning from zero to 2 kG. Under these extreme conditions, all diagnostic techniques employed in quiet Sun magnetometry are strongly biased towards a particular range of field strengths, and the Mn I signals are not expected to be the exception. Consequently, the diagnostic content of the Mn I lines cannot be fully exploited unless their biases are properly understood. Such task is undertaken in the paper by exploring the response of Mn I lines in a number of realistic quiet Sun scenarios.

Three complementary LTE synthesis codes have been written and tested (ME, 1D and MISMA; § 2). They provide a number of relevant results, the first one being the ability to reproduce all observed Mn I HFS patterns. We reproduce the observed unpolarized line profile of nine assorted lines corresponding to all HFS sensitivities (§ 6). The study is focused on the line most often used in magnetometry, Mn I 5538, however its behavior should be representative of the other lines. According to the weak magnetic field approximation, the Stokes V signals scale with the longitudinal component of the magnetic field, i.e., the magnetic field strength times the cosine of the magnetic field inclination with respect to the LOS. We verify that the scaling on cosine holds very tightly. The scaling on the magnetic field strength, however, breaks down soon (when $B \geq 400$ G for Mn I 5538). Even for ME atmospheres, the weak field approximation predicts a Stokes V signal twice as large as the synthetic one for $B \simeq 1.5$ kG. When the expected coupling between the thermodynamic conditions and the magnetic field strengths is taken into account, the dimming of the kG Stokes V signals can be as large as two orders of magnitude (see Figs. 3 and 8). The dimming of the polarization signals formed in kG magnetic concentrations affects all Mn I lines (§ 3), and it has significant observational implications.

If the resolution elements contains both weak and strong fields, then the kG fields tend to be under-represented in the average profile. We have modelled the bias assuming a multi component atmosphere, where the synthetic signals are weighted means of the Stokes profiles corresponding to each single field strength. The weight is given by the fraction of atmosphere filled by each field strength, i.e., by the magnetic field strength probability density function PDF (equations [4] and [5]). According to our modeling, even when the (un-

signed) magnetic flux and the magnetic energy are dominated by kG magnetic fields, the Stokes V profile of Mn I $\lambda 5538$ can show HFS reversal at line core characteristic of hG fields (Fig. 7). A pure morphological inspection of the Stokes profiles does not suffice to infer which is the dominant magnetic field strength in the resolution element. For the HFS hump of Mn I $\lambda 5538$ to disappear the kG filling factor has to be larger than the sub-kG filling factor and, consequently, when the HFS hump disappears the magnetic flux and magnetic energy of the atmosphere are completely dominated by kG fields (§ 4.1).

Detecting Stokes V profiles with HFS features indicates the presence of hG fields in the resolution element. However, this sole observation does not tell whether the hG field strengths dominate. There seem to be two extreme alternatives to exploit the diagnostic potential of these lines. First, improving the spatial resolution of the observations to a point where the quiet Sun magnetic structures can be regarded as spatially resolved. Unfortunately, this possibility does not seem to be feasible at present. Realistic simulations of magneto-convection indicate that quiet Sun magnetic fields are uniform only at the diffusive length scales (e.g. Cattaneo 1999; Vögler & Schüssler 2007), which are

of the order of a few km in the photosphere (e.g. Schüssler 1986). These scales are very far from the angular resolution of the present measurements, and even much smaller than the length-scale for the radiative transfer average along the LOS (Sánchez Almeida et al. 1996). We prefer the alternative possibility, namely, developing inversion techniques where complex magnetic atmospheres are included into the diagnostics. Using appropriate constraints, the number of free parameters required to describe such atmospheres can be maintained within reasonable limits (e.g., the model MISMA's in Sánchez Almeida 1997). Dealing with unresolved velocities also favors detailed inversion codes (§ 5). We are presently working on these improvements needed to develop the diagnostic technique pioneered by López Ariste et al..

We thank Arturo López Ariste and Rafael Manso for helpful discussions during the development of this work. BV acknowledges a grant from the *Università Tor Vergata* while visiting the IAC. This work has been partly funded by the Spanish Ministry of Education and Science (project AYA2004-05792).

REFERENCES

- Asensio Ramos, A., Martínez González, M. J., López Ariste, A., Trujillo Bueno, J., & Collados, M. 2007, *ApJ*, 659, 829
 Bellot Rubio, L. R., & Collados, M. 2003, *A&A*, 406, 357
 Blackwell-Whitehead, R. J., Pickering, J. C., Pearse, O., & Nave, G. 2005, *ApJS*, 157, 402
 Bomnier, V., Derouich, M., Landi Degl'Innocenti, E., Molodij, G., & Sahal-Bréchet, S. 2005, *A&A*, 432, 295
 Cattaneo, F. 1999, *ApJ*, 515, L39
 Domínguez Cerdá, I., Sánchez Almeida, J., & Kneer, F. 2003, *A&A*, 407, 741
 —. 2006a, *ApJ*, 636, 496
 —. 2006b, *ApJ*, 646, 1421
 Emonet, T., & Cattaneo, F. 2001, *ApJ*, 560, L197
 Faurobert, M., Arnaud, J., Vigneau, J., & Frish, H. 2001, *A&A*, 378, 627
 Faurobert-Scholl, M. 1993, *A&A*, 268, 765
 Fisher, R. A., & Peck, E. R. 1939, *Phys. Rev.*, 55, 270
 Khomenko, E. V., Collados, M., Solanki, S. K., Lagg, A., & Trujillo-Bueno, J. 2003, *A&A*, 408, 1115
 Landi Degl'Innocenti, E. 1975, *A&A*, 45, 269
 —. 1976, *A&AS*, 25, 379
 —. 1978, *A&AS*, 33, 157
 Landi Degl'Innocenti, E., & Landolfi, M. 2004, *Astrophysics and Space Science Library*, Vol. 307, Polarization in Spectral Lines (Dordrecht: Kluwer)
 Lefèvre, P.-H., Garnier, H.-P., & Biémont, E. 2003, *A&A*, 404, 1153
 Lin, H., & Rimmele, T. 1999, *ApJ*, 514, 448
 Lites, B. W. 2002, *ApJ*, 573, 431
 López Ariste, A., Martínez González, M. J., & Ramírez Vélez, J. C. 2007, *A&A*, 464, 351
 López Ariste, A., Tomczyk, S., & Casini, R. 2002, *ApJ*, 580, 519
 —. 2006, *A&A*, 454, 663
 Maltby, P., Avrett, E. H., Carlsson, M., Kjeldseth-Moe, O., Kurucz, R. L., & Loeser, R. 1986, *ApJ*, 306, 284
 Margrave, Jr., T. E. 1972, *Sol. Phys.*, 27, 294
 Martínez González, M. J., Collados, M., & Ruiz Cobo, B. 2006, *A&A*, 456, 1159
 Moore, C. E., Minnaert, M. G. J., & Houtgast, J. 1966, *The Solar Spectrum from 2935 Å to 8770 Å*, NBS Mono. 61 (Washington: NBS)
 Neckel, H. 1999, *Sol. Phys.*, 184, 421
 Ralchenko, Y., Jou, F.-C., Kelleher, D., Kramida, A., Musgrove, A., Reader, J., Wiese, W., & Olsen, K. 2007, *NIST Atomic Spectra Database (version 3.1.2)* (Gaithersburg, MD: National Institute of Standards and Technology), <http://physics.nist.gov/asd3>
 Sánchez Almeida, J. 1992, *Sol. Phys.*, 137, 1
 —. 1997, *ApJ*, 491, 993
 Sánchez Almeida, J. 1998, in *ASP Conf. Ser.*, Vol. 155, Three-Dimensional Structure of Solar Active Regions, ed. C. E. Alissandrakis & B. Schmieder (San Francisco: ASP), 54
 —. 2000, *ApJ*, 544, 1135
 Sánchez Almeida, J. 2004, in *ASP Conf. Ser.*, Vol. 325, The Solar-B Mission and the Forefront of Solar Physics, ed. T. Sakurai & T. Sekii (San Francisco: ASP), 115, (astro-ph/0404053)
 —. 2005, *A&A*, 438, 727
 Sánchez Almeida, J., Emonet, T., & Cattaneo, F. 2003, *ApJ*, 585, 536
 Sánchez Almeida, J., Landi Degl'Innocenti, E., Martínez Pillet, V., & Lites, B. W. 1996, *ApJ*, 466, 537
 Sánchez Almeida, J., & Lites, B. W. 2000, *ApJ*, 532, 1215
 Sánchez Almeida, J., & Trujillo Bueno, J. 1999, *ApJ*, 526, 1013
 Schrijver, C. J., & Title, A. M. 2003, *ApJ*, 597, L165
 Schüssler, M. 1986, in *Small Scale Magnetic Flux Concentrations in the Solar Photosphere*, ed. W. Deinzer, M. Knölker, & H. H. Voigt (Göttingen: Vandenhoeck & Ruprecht), 103
 Socas-Navarro, H., Martínez Pillet, V., & Lites, B. W. 2004, *ApJ*, 611, 1139
 Socas-Navarro, H., & Sánchez Almeida, J. 2002, *ApJ*, 565, 1323
 —. 2003, *ApJ*, 593, 581
 Solanki, S. K. 1986, *A&A*, 168, 311
 Solanki, S. K., & Steenbock, W. 1988, *A&A*, 189, 243
 Spruit, H. C. 1976, *Sol. Phys.*, 50, 269
 Stein, R. F., & Nordlund, Å. 2006, *ApJ*, 642, 1246
 Stenflo, J. O. 1982, *Sol. Phys.*, 80, 209
 Trujillo Bueno, J., Shchukina, N. G., & Asensio Ramos, A. 2004, *Nature*, 430, 326
 Unno, W. 1959, *ApJ*, 129, 375
 Vögler, A., Shelyag, S., Schüssler, M., Cattaneo, F., Emonet, T., & Linde, T. 2005, *A&A*, 429, 335
 Vögler, A. 2003, PhD thesis, Göttingen University, Göttingen
 Vögler, A., & Schüssler, M. 2003, *Astron. Nachr.*, 324, 399
 Vögler, A., & Schüssler, M. 2007, *A&A*, 465, L43
 Yi, Z., Jensen, E., & Engvold, O. 1993, in *ASP Conf. Ser.*, Vol. 46, The Magnetic and Velocity Fields of Solar Active Regions, ed. H. Zirin, G. Ai, & H. Wang, San Francisco, 232

APPENDIX

MULTI-COMPONENT ATMOSPHERE WITH MAGNETIC FIELD VECTORS VARYING IN DIRECTION

The equations (4) and (5) used for multi-component syntheses hold even when the magnetic field vector presents a distribution of magnetic field inclinations, θ , and magnetic field azimuths, ϕ . In the general case the PDF depends on B , θ and ϕ , $\mathcal{P}(B, \theta, \phi)$,

so that the average Stokes I and Stokes V profiles are,

$$I = \int_0^{2\pi} \int_0^\pi \int_0^{B_{\max}} \mathcal{P}(B, \theta, \phi) S_I(B, \theta, \phi) dB d\theta d\phi, \quad (\text{A1})$$

$$V = \int_0^{2\pi} \int_0^\pi \int_0^{B_{\max}} \mathcal{P}(B, \theta, \phi) S_V(B, \theta, \phi) dB d\theta d\phi, \quad (\text{A2})$$

with $\mathcal{P}(B, \theta, \phi)$ normalized to one. The symbols $S_I(B, \theta, \phi)$ and $S_V(B, \theta, \phi)$ stand for the Stokes I and V profiles corresponding to each magnetic field vector. As the tests carried out in § 3 show, and as it is to be expected from the weakly polarizing medium approximation (Sánchez Almeida & Trujillo Bueno 1999), the intensity of the weak Mn I lines is independent of inclination and azimuth so that $S_I(B, \theta, \phi) \simeq I_B$. Similarly, Stokes V is independent of ϕ and depends on θ through the factor $\cos \theta$, $S_V(B, \theta, \phi) = V_B \cos \theta$. The symbol V_B represents the Stokes V profile for longitudinal magnetic field ($\cos \theta = 1$). Then from equations (A1) and (A2) one retrieves the equations (4) and (5) used in the main text,

$$I = \int_0^{B_{\max}} P(B) I_B dB, \quad (\text{A3})$$

$$V = \int_0^{B_{\max}} \langle \cos \theta \rangle P(B) V_B dB, \quad (\text{A4})$$

with

$$P(B) = \int_0^{2\pi} \int_0^\pi \mathcal{P}(B, \theta, \phi) d\theta d\phi, \quad (\text{A5})$$

and

$$\langle \cos \theta \rangle = \frac{1}{P(B)} \int_0^{2\pi} \int_0^\pi \cos \theta \mathcal{P}(B, \theta, \phi) d\theta d\phi. \quad (\text{A6})$$